

Cone beam X-ray scatter removal via image frequency modulation and filtering

Jonathan S Maltz, Wolf-Ekkehard Blanz, Dimitre Hristov and Ali Bani-Hashemi

Abstract—We present a novel method for rapid removal of patient scatter from cone beam (CB) projection images that requires no scatter measurement, physical modeling or strong assumptions regarding the spatial smoothness of the scatter distribution. **Method:** A modulator grid is placed between the imaged distribution and the detector that differentially frequency modulates primary and scattered photons. When photons travel through the grid, photons that originate directly from the CB source are modulated by a higher frequency than scattered photons that have more proximal, diffusely distributed sources. We employ non-linear Fourier domain filtering to attenuate the contribution of scatter to the image spectrum. The theoretical validity of the method is verified using linear analysis of planar sources and its performance is evaluated using a simulator based on this analytical model. **Results:** Simulation experiments with an ideal modulator indicate that even unrealistically large amounts of scatter are almost entirely removed by this method. The recovered images are devoid of major artifacts and exhibit an RMS error of 10%. **Conclusions:** We have verified the theoretical validity of scatter removal via spatial frequency modulation. A disadvantage of the technique is that it will always produce a filtered image having at best 0.41 of the maximum detector resolution when maximum scatter rejection is desired. This is not a major consideration in most medical X-ray CB imaging applications using contemporary detector technology, especially since scatter often significantly reduces useful resolution.

I. INTRODUCTION

Cone beam projection imagers offer increased simultaneous field-of-view over fan beam based systems. This is especially important for applications involving fluoroscopy, radiation therapy and in dynamic CT (4D) studies where tissue motion and contrast agent flow must be recovered from a set of time-gated projections. Also, the routine use of X-ray CT for diagnostic purposes is currently limited by the large radiation dose of full-body scans. Cone beam systems allow for more efficient collection of photons and hence for lower dose rates. However, the lack of collimation leads to large amounts of scatter which decreases the attractiveness of general diagnostic cone beam CT (CBCT) systems.

Many methods of scatter reduction and compensation have been proposed in the past. Most methods are based on simplified models of scatter physics, simplified geometrical descriptions of the imaged distribution, or make assumptions relating to the smoothness of the scatter distribution in the projection images [1], [2], [3]. Full Monte Carlo simulation methods are too time consuming for practical use in real-time imaging applications [4]. Beam-stop arrays can be used

to measure scatter directly, but require the acquisition of two sets of projection images, which is inconvenient [5]. We present a method that makes no assumptions regarding the imaged distribution (other than limited bandwidth), imposes low computational burden, and requires no increase in the number of acquired images.

II. MODULATION SCHEME FOR PLANAR OBJECT AND SOURCES

Consider a planar source distribution $s(x,y)$. A planar object $t(x,y)$ is placed at distance d_0 from the source along the z -axis. At a distance $d_1 \geq d_0$ is the modulator plane $t_m(x,y)$ and the detector lies at $z = d_2 \geq d_1$.

Consider the modulator plane transmission function supported on $x,y \in [-W,W]$:

$$t_m(x,y,z = d_1) = A \left[B + \cos(2\pi u_0 x + v_0 y) \right] \times \text{rect}\left(\frac{x}{W}, \frac{y}{W}\right). \quad (1)$$

where u_0 and v_0 are the horizontal and vertical frequencies, respectively. The cosine is chosen with orientation along the image diagonal as this allows modulation to be performed closest to the maximum frequency that can be represented in the image. This in turn maximizes the resolution of the recovered image.

For those photons arriving at the modulator from the source (unscattered photons), we may translate the modulator to the object plane. During this translation, demagnification by:

$$M' = \frac{d_1}{d_0}$$

occurs giving:

$$t'_m(x,y,z = d_0) = A \left[B + \cos(2\pi M'(u_0 x + v_0 y)) \right] \times \text{rect}\left[\frac{x}{W/M'}, \frac{y}{W/M'}\right].$$

The image that forms from the direct unscattered photons is then:

$$i_d(x,y) = \frac{1}{4\pi d_2^2 m_2^2} s\left(\frac{x}{m_2}, \frac{y}{m_2}\right) * \left[t\left(\frac{x}{M_2}, \frac{y}{M_2}\right) t'_m\left(\frac{x}{M_2}, \frac{y}{M_2}\right) \right]$$

where:

$$M_2 = \frac{d_2}{d_0}, \quad m_2 = -\frac{d_2 - d_0}{d_0} = 1 - M_2$$

and the operator “*” denotes 2D convolution.

This work was supported by Siemens Medical Solutions USA, Inc. The authors are with the Oncology Care Systems Group, Siemens Medical Solutions USA, Inc., 4040 Nelson Ave, Concord CA 94520, jonathan.maltz@siemens.com

The Fourier transform of this image is:

$$\begin{aligned}
I_d(u, v) &= \frac{1}{4\pi d_2^2 m_2^2} m_2^2 S(m_2 u, m_2 v) M_2^2 \times \\
&\quad [T(M_2 u, M_2 v) * T'_m(M_2 u, M_2 v)] \\
&= \frac{A M_2^2 W^2}{4\pi d_2^2 M'^2} S(m_2 u, m_2 v) \left\{ T(M_2 u, M_2 v) * \right. \\
&\quad \left[\left(B \delta(u, v) + \right. \right. \quad (2) \\
&\quad \left. \left. \delta(u \pm u_0 M'/M_2, v \pm v_0 M'/M_2)/2 \right) * \right. \\
&\quad \left. \left. \text{sinc}\left(\frac{W M_2}{M'} u, \frac{W M_2}{M'} v\right) \right] \right\} \quad (3)
\end{aligned}$$

Now we consider the scatter image. We assume that each point in the image is an isotropic scatter source giving:

$$o(x, y) = \alpha(1 - t(x, y))$$

where α is an efficiency factor that is assumed equal for all sources on the object plane. The scatter image is then:

$$i_s(x, y) = \frac{\alpha}{4\pi(d_2 - d_0)^2 m_1^2} \left[1 - t\left(\frac{x}{m_1}, \frac{y}{m_1}\right) \right] * t_m\left(\frac{x}{M_1}, \frac{y}{M_1}\right)$$

where

$$M_1 = \frac{d_2 - d_0}{d_1 - d_0} = \frac{M_2 - 1}{M' - 1}$$

and

$$m_1 = \frac{d_2 - d_1}{d_1 - d_0} = \frac{M_2 - M'}{M' - 1}.$$

This has the Fourier transform:

$$\begin{aligned}
I_s(x, y) &= \frac{\alpha}{4\pi(d_2 - d_0)^2 m_1^2} \left[\delta(u, v) - m_1^2 T(m_1 u, m_1 v) \right] \times \\
&\quad T_m(M_1 u, M_1 v) \\
&= \frac{A \alpha W^2}{4\pi d_2^2 m_1^2} \left[\delta(u, v) - m_1^2 T(m_1 u, m_1 v) \right] \times \\
&\quad \left[\text{sinc}(W u, W v) * \right. \\
&\quad \left. \left(B \delta(u, v) + \delta(u \pm u_0/M_1, v \pm v_0/M_1)/2 \right) \right]. \quad (4)
\end{aligned}$$

Comparing the expressions for the FTs of the direct image i_d (2) and scatter image i_s (4), we see that the former is modulated to the coordinates $(\pm u_0 M'/M_1, \pm v_0 M'/M_1)$ on the Fourier plane while the latter is *multiplied* by the final factor in (4). The fact that this is a multiplication rather than a convolution stems from the diffuse, unfocused nature of the source. The spectrum I_s will have magnitude peaks at the origin and around $(\pm u_0/M_1, \pm v_0/M_1)$. Since $M'/M_2 > 1/M_1$, the direct image is modulated to frequency that is higher than the peak of the scatter spectrum. These two mechanisms enable the efficient removal of scatter.

III. SIMULATION AND RESULTS

We now demonstrate the ability of the method to remove scatter from the contaminated image shown in Figure 1. We consider a CB imaging system having a realistic geometry in which the source-to-object distance $z = d_0 = 0.85\text{m}$, the modulator plane is at $z = d_1 = 1.25\text{m}$ and the detector lies at $z = d_2 = 1.40\text{m}$. The detector has 1024 pixels per side length of 0.4m.

While we simulate using a planar object, we note that the ability to remove scatter is based on the separation along the z -axis of the cone source and the scatter sources. The performance is thus limited by the distance between the cone source and the most proximal object plane. We have thus chosen an object plane 15cm proximal to the source from the imaging system isocenter. All object planes distal to this plane will appear closer to the origin of the spectrum and their scatter contributions will consequently will not limit the performance of this method.

In order to make maximum use of the available detector bandwidth, we wish to modulate the spectrum by the maximum amount possible. The maximum horizontal and vertical frequencies that can be recorded by this detector are $u_n = v_n = 1280$ line-pairs per meter (lp/m). As shown in Figure 2, we can at most fit the image baseband spectrum and 2 modulated copies along the diagonal of the frequency plane. This limits the maximum image bandwidth to $\rho_d = 1/(\sqrt{2} + 2)u_n \approx 0.4142u_n = 530.19$ lp/m. This constitutes a reasonable bandwidth for medium to high quality medical X-ray images. The object in Figure 1 contains a jinc function $(J_1(\pi r))/2r$, where J_1 is a Bessel function of the first kind), which has uniform radial frequency content. This makes the spectral support of the primary image more easily visible. The modulator frequency is fully determined by the above analysis with $u_0 = v_0 = (d_2/d_1)\sqrt{2}\rho_d = 839.78$ lp/m. In the detector plane, the effective modulator frequency is $u_m = v_m = \sqrt{2}\rho_d = 749.81$ lp/m.

The spectral peaks for the scatter originating at the plane at $z = d_0$ lie at $u_s = v_s = \pm u_0/M_1 = \pm 610.75$ lp/m. These fall within quadrant III of the modulated image spectrum at (u_m, v_m) and quadrant I of that at $(-u_m, -v_m)$. These quadrants consequently suffer significant corruption from scatter. However, since i_d is real, we may reconstruct either quadrant by exploiting the conjugate symmetry of the Fourier transform and the fact that the other 3 quadrants are not significantly affected. Before an image spectrum (say the copy at (u_m, v_m) , which we denote $F_m(u, v)$) is reconstructed, it is copied to a clean Fourier plane and restored to baseband using the Fourier shift theorem: $F_r(u, v) = F_m(u, v) e^{j2\pi(-u_m x - v_m y)}$. Information from quadrants I, II and IV is used to create a spectrum of a real image. This is then inverse Fourier transformed to yield the filtered image $f_r(x, y)$. Figure 4 shows that the reconstructed image contains no visible traces of scatter. Resolution is slightly reduced, and some minor artifacts are visible. We quantify the RMS

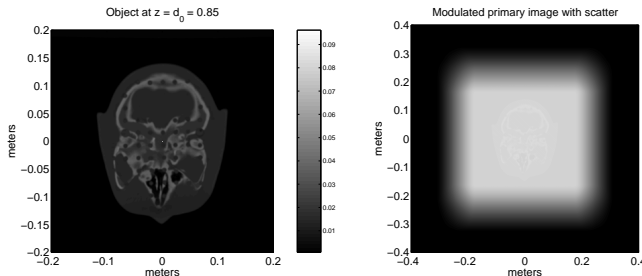


Fig. 1. The left figure shows the true planar object while right shows the same object plus simulated isotropic scatter.

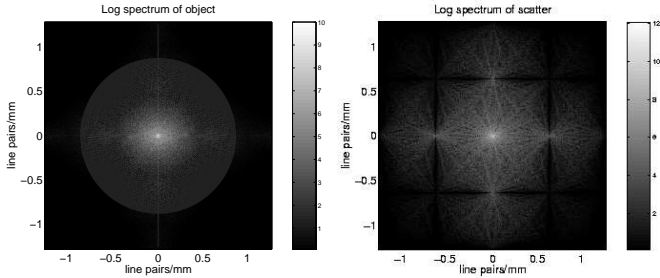


Fig. 2. Left: Log magnitude spectrum of the object shown at left of Figure 1. Right: Log magnitude spectrum of scatter image.

percentage error as:

$$E = \frac{\sqrt{\sum_i (f_r^i - f^i)^2}}{\sqrt{\sum_i (f^i)^2}} \times 100$$

where f_r^i and f^i are the i th pixels of the recovered and original object images, respectively. For this example, we find $E = 10.44\%$. This is consistent with the subjective evaluation of the reconstructed image and the small amplitude of the absolute difference image at the right of Figure 4.

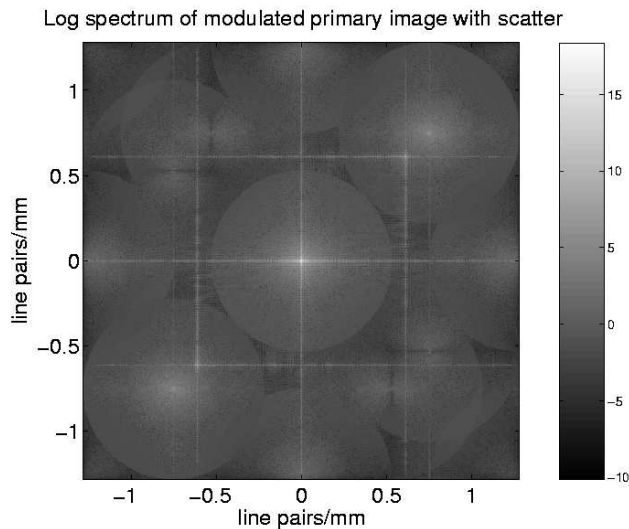


Fig. 3. Log magnitude spectrum of the object shown at right of Figure 1 after modulation. Note the scatter spectral peaks that appear on the diagonal between the baseband spectral copy and the modulated image spectral copies.

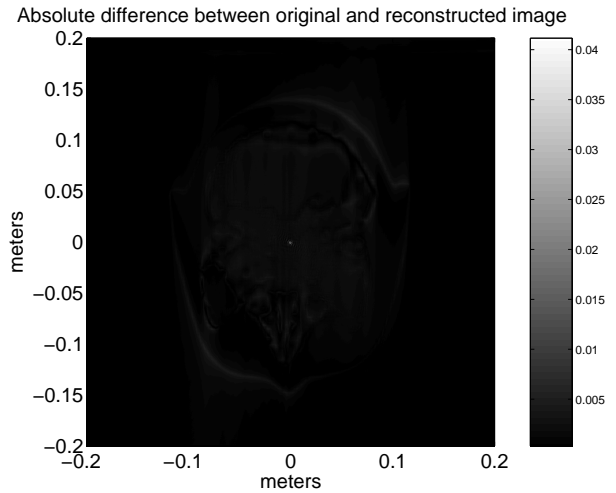
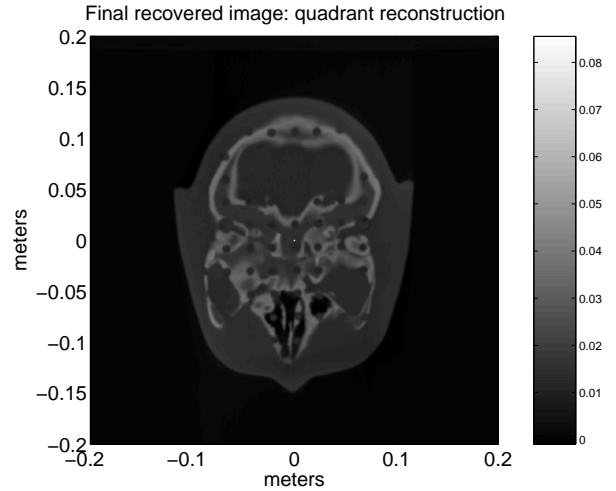


Fig. 4. Upper: Image from which scatter has been removed. Lower: Absolute difference image between true and recovered images.

IV. CONCLUSION

The performance of the modulator in these preliminary simulations is very encouraging and motivates for the implementation this method. Before this is possible, numerous practical concerns must be addressed. In X-ray imaging, we are normally concerned with generating images that consist of attenuation maps of the imaged distribution. However, in our modulation scheme, it is the photon fluence that must be modulated using an attenuating modulator. Consider the fluence along a single ray incident at the detector:

$$\phi(x, y) = \phi_0 e^{-\int_L \mu(x, y, z) dl}$$

Here, ϕ_0 is the fluence originating at the cone source that traverses the imaged distribution along the path L . The attenuation distribution of the imaged object is denoted as $\mu(x, y, z)$. Since fluence is physically non-negative, we must multiply $\phi(x, y)$ by t_m in (1) and ensure $B \geq 1$:

$$\phi_m(x, y) = \phi_0 e^{-\int_L \mu(x, y, z) dl} A [B + \cos(2\pi u_0 x + v_0 y)].$$

Since the modulator is attenuating, $A \leq 1$. The maximum fractional modulation is achieved for $B = 1$. Let $\tau(x, y)$

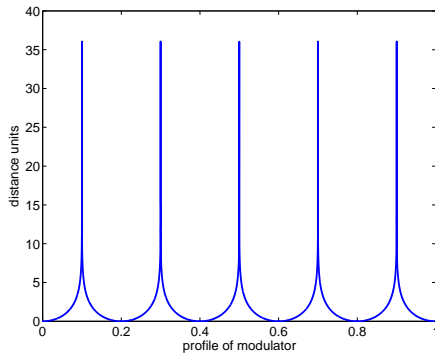


Fig. 5. Shape of the modulator profile.

represent the spatially-varying thickness (along the z-axis) of the physical modulator. To produce the desired modulation we must have:

$$\tau(x, y) = -\ln(1/2[1 + \cos(2\pi u_0 x + v_0 y)]) / \mu_m$$

where μ_m is the density of the modulator material. Since $\tau(x, y) \geq 0$, the argument of the logarithm must be in the interval $(0, 1]$ and thus $A = 1/2$ for optimal modulation. Figure 5 illustrates the modulator profile. The effects of the singularities in $\tau(x, y)$ are reduced by adding a small positive number to the argument of the logarithm. We expect the fabrication of a modulator having this profile to pose practical difficulties that may be surmounted using multilayer material patterning and lamination technologies.

The above analysis ignores the obliquity of rays incident on the modulator. For this reason, the device should be designed to be as thin as possible.

REFERENCES

- [1] L. A. Love and R. A. Kruger, "Scatter estimation for a digital radiographic system using convolution filtering," *Med Phys*, vol. 14, no. 2, pp. 178–85, Mar-Apr 1987.
- [2] B. Ohnesorge, T. Flohr, and K. Klingensbeck-Regn, "Efficient object scatter correction algorithm for third and fourth generation ct scanners," *European Radiology*, vol. 9, pp. 563–569, March 1999.
- [3] L Spies, M Ebert, B A Groh, B M Hesse, and T Bortfeld, "Correction of scatter in megavoltage cone-beam ct," *Physics in Medicine and Biology*, vol. 46, no. 3, pp. 821–833, 2001.
- [4] Colijn AP and Beekman FJ, "Accelerated simulation of cone beam X-ray scatter projections," *IEEE Trans Med Imaging*, vol. 23, no. 5, pp. 584–590, MAY 2004.
- [5] R. Ning, X. Tang, and D. Conover, "X-ray scatter correction algorithm for cone beam CT imaging," *Med Phys*, vol. 31, no. 5, pp. 1195–202, may 2004.